A Photoactive Ag(I) Based Coordination Polymer as a Potential Semiconductor for Photocatalytic Water Splitting and Environmental Remediation: Experimental and Theoretical Approach

*Subrata Mandal[1], Sachin P. Nanavati[2], David J. Willock[2] and Rajakumar Ananthakrishnan[1]**

[1]Department of Chemistry, Environmental Materials & Analytical Chemistry Laboratory, Indian Institute of Technology, Kharagpur 721302, India
E-mail: raja.iitchem@yahoo.com; Fax: +91 3222-282252; Tel: +91 3222 282322

[2]Cardiff Catalysis Institute, School of Chemistry, Cardiff University, Cardiff, CF10 3AT, UK.

ABSTRACT Metal organic frameworks (MOFs) or Metal coordination polymers (CPs) with controlled structure on the micro/nano-scale have attracted intense interest for potential applications in a wide variety of fields, such as energy storage and conversion, chemical and biological sensing, and catalysis. Here, we report a new class of photocatalytic material, Ag(I) based nano-micro structured coordination polymer (Ag(I)-CP), which offer performance at a level competitive with known semiconductors in photocatalytic water oxidation and oxidation of organic compounds, such as dye/ organic pollutants present in contaminated water. The coordination polymer was synthesized by a wet-chemical route and has been characterized using powder X-ray diffraction, X-ray photoelectron spectroscopy and electron microscopy. The

Ag(I)-CP has notable semiconducting characteristics and charge transfer ability due to ligand centered charge transfer (LCCT) in combination with metal to ligand charge transfer MLCT (Ag-O cluster to ligand centre) as established from experimental absorption, luminescence and photoelectrochemical measurements alongside DFT calculations. Notably, Ag(I)-CP exhibits a highly reactive valance band potential +3.40 V *vs* NHE, composed of hybridized state of O *2p* and C *2p* through the organic linker and Ag *4d*, this acts as an active center for the generation of reactive oxygen species (ROS) *i.e.,* hydroxyl radical and h^+ under photocatalytic conditions. Consequently, the photogenerated species facilitate effective oxidations of water and organic contaminants such as tartrazine, rhodamine B and 2, 4-dichlorophenol under UV light irradiation. Furthermore, our results suggest that the Ag(I)-CP could be used as a promising material for the development of heterostructure for variety of photo-assisted-redox catalysis.

INTRODUCTION

Photocatalysis finds important applications for the oxidation of organic pollutants in industrial water streams and for solar-energy conversion via water splitting. The pioneering work of Fujishima and Honda on TiO_2 in 1972, led researchers engaged in the applications of semiconductor materials, such as TiO_2, ZnO, CdS, *etc*. to turn to the field of photocatalysis.[1, 2] However, such classical semiconductor based materials are not suited to large-scale application in photocatalysis due to poor efficiencies resulting from limited surface area (low surface to volume ratios), short life time of the charge carriers and low charge conductivity. Hence, developing a new-generation heterogeneous photocatalysts became an important research task. Recently, metal coordination polymer (CPs)/ metal organic frameworks (MOFs) have offered new material design options to engineer structural and electronic properties in a flexible manner.

These materials have intriguing features such as uniform porous structures and tunable functionalities. MOFs are crystalline solids are built up from metal-oxide clusters interconnected by organic linkers and so provide a suitable platform for host-guest interactions.[3,4]Unlike classical semiconductors, charge transport phenomenon and the separation of active h^+/e^- in MOFs/CPs is greatly influenced by two discrete components (inorganic nodes and organic linkers) which offers the opportunity to tune the material properties.[5] In particular, the work of Garcia *et al.*[6] and Férey *et al.*[7] on photoactive MOF-5 and MIL-125(Ti), respectively, revealed that these new-classes of semiconductor could be used in the field of photovoltaics/ photocatalysis. A sub-field of research has thus emerged with the aim of synthesizing new MOF/CP based semiconductor materials with tuned optical response produced by modifying the inorganic unit or the organic linker (length and chemical functionalization) through either synthetic and/or computational screening programmes.[8,9]Although interesting properties have been obtained the basic understanding of how the material composition and structure brings about the optical and semiconducting behavior is still a matter of debate. For example, the charge transfer process of MOF-5 is still controversial as Qiu *et al.* revealed it is LLCT[10] rather than LMCT[6] using relativistic density functional theory and time dependent DFT. So far, then, understanding of the mechanism of the charge separation process and semiconducting behavior of the MOF/CPs is at a relatively early stage. Hence, designing a new class of CPs/MOFs and investigating their band structure with respect to change of metal nodes by a combined experimental and computational approach would help to develop a more reliable understanding of the origin of photocatalytic properties.[9, 11]Notably, CPs containing Ag(I) can give a versatile class of materials distinct from transition metal-based materials through the characteristic features of the Ag(I) cation, such as coordination adaptability and metal-metal interaction.[12,

[13]Usually, Ag(I) based semiconductors such as Ag_2O, Ag_3PO_4, Ag_3AsO_4, *etc.* are found to be effective in photocatalysis.[14, 15, 16] However, their low-lying hybridized 5*s*-5*s* states and/or 5*s*/5*p*-4*d* states of silver in the conduction band minimum (CBM) facilitate the reduction of lattice Ag^+ resulting in a high level of photo-leaching.[14, 15] Additionally, low surface area and stability, prevent large-scale use of these simple compounds for photocatalytic applications.[14,17] CPs/MOFs of Ag(I) with suitable organic linkers can provide an alternative strategy to design highly active photocatalytic materials. Ag(I)-CPs can be formed using 1, 4-benzene dicarboxylic acid (H_2bdc) as linker. H_2bdc takes on a bidentate coordination mode in Ag(I)-CP, which should lead to improved stability of the Ag(I) species and so this approach has been used in our research to synthesize a Ag(I)-CP material and to investigate its photochemical properties.

Herein we describe the synthesis of a nano-micro structured Ag(I) coordination polymer (Ag(I)-CP) using a H_2bdc linker and experiments to explore the application of Ag(I)-CP as a new class of photocatalytic material for the oxidation of organic contaminants such as tartrazine, rhodamine B, and 2, 4 dichlorophenol in water. Detail investigation of the photochemical and photophysical properties of the Ag(I)-CP in combination with electronic structure calculated by density functional theory suggests that Ag(I)-CP exhibits semiconducting behavior and undergoes a ligand centered (LCCT) accompanied with metal to ligand (MLCT) charge transfer process. We find that a highly reactive hole with a potential +3.40 V vs NHE is generated after excitation in UV light and propose that either the hole itself, or hydroxyl radicals generated when this hole interacts with water, are responsible for the observed high photocatalytic activity. Noteworthy, our Ag(I)-CP photocatalyst is capable to oxidize tartrazine under simulated sunlight due to its UV active catalytic behavior in combination with sensitization of tartrazine from visible light region.

EXPERIMENTAL SECTION

Chemicals and materials

1, 4-benzenedicarboxylic acid (H_2bdc) was obtained from Central Drug House (P) Ltd. (India). Silver nitrate was obtained from Sigma Aldrich. All other chemical reagents utilized in the present work were analytical grade, purchased from Merck Specialties Private Limited and used without further purification. Deionized water was used throughout.

Synthesis of Ag(I)-CP

Ag(I)-CP was synthesized using the required stoichiometric amount of the precursor. In brief, 2 mmol of $AgNO_3$ was mixed in 10 mL aqueous ammonia solution (10 M) and stirred for 1 h, a transparent solution formed following reaction (1). Meanwhile, 1 mmol of H_2bdc was dissolved in 15 mL of water to form an aqueous solution to which 0.2 mL of 25% NH_3 was added. The dissolved H_2bdc was combined with the $AgNO_3$ solution and the resulting mixture was continuously stirred for 2 h before the final solid product, Ag(I)-CP produced following reaction (2), could be collected by centrifugation. The product was washed with deionized water and ethanol several times. The recovered solid powder was dried in an oven at 60° C for 12 h.

$$AgNO_3 + 2NH_4OH \rightarrow [Ag(NH_3)_2]^+ + NO_3^- + 2H_2O \quad (1)$$

$$[Ag(NH_3)_2]^+ + H_2bdc \rightarrow \quad Ag(I)\text{-}CP\downarrow + 2NH_4^+ \quad (2)$$

Synthesis of Ag_2O, CuO, TiO_2 and ZnO

To allow comparison of the photocatalytic activity of Ag(I)-CP with well-known light active semiconductors Ag_2O, CuO, TiO_2, ZnO materials were prepared following literature reported procedures[18, 19, 20] and further characterized by powder X-ray diffraction pattern as shown in Figure S4a.

Characterizations

The Fourier Transform Infra-Red spectrum of the Ag(I)-CP was recorded with a Perkin-Elmer FT-IR spectrophotometer RXI. The X-ray diffraction (XRD) pattern of Ag(I)-CP was obtained using a BRUKER-AXS-D8-ADVANCE diffractometer with Cu Kα radiation (λ = 1.5418 Å) in the 2θ range 5°-90° at a scan rate of 0.5° min^{-1}. X-ray Photoelectron Spectroscopy (XPS) was performed by Specs (Germany) to investigate the surface atomic composition and oxidation state of the elements present in the Ag(I)-CP. Electron Microscopy (FESEM) is used for morphological characterization of the Ag(I)-CP using a microscope accelerating voltage of 5 kV (NOVA NANOSEM 450). TEM images were obtained by JEOL JEM-2100 transmission electron microscopes, elemental mapping and dark field imaging is done in STEM mode with HAADF detector. TEM Samples were prepared by dropping a few samples dispersed in ethanol on carbon-coated 200 mesh copper grids. BET surface area and N_2 sorption isotherms (77K) of the prepared Ag(I)-CP was carried out by using Micromeritics ASAP 2020. For adsorption-desorption study the sample was degassed overnight and 50 mg was loaded in a 6 mm sample holder. Brunauer–Emmett–Teller (BET) calculations are performed for the analysis of surface area of the sample. UV–Vis diffuse reflectance spectra (UV–Vis DRS) were obtained by a Cary 500 UV–Vis spectrophotometer using $BaSO_4$ powder as an internal standard. Photoluminescence emission and excitation spectra of the prepared Ag(I)-CP and ligand were recorded by Horiba fluorolog-3 (solid state). In addition Ag(I)-CP sample before and after use in photocatalytic process were excited at 325 nm to investigate the change in recombination rate of hole and electron upon light irradiation.

Photoelectrochemical measurements

An electrochemical station is used to measure photocurrent using a three-electrode mode with 0.5 M Na_2SO_4 solution (pH = 7.0) as the electrolyte. In brief, 10 mg of Ag(I)-CP was added to 1

mL of ethanol. The as-prepared solution was stirred for 30 min to ensure that the Ag(I)-CP was uniformly dispersed in the solution. 10 μL of the 10 mg mL^{-1} Ag(I)-CP solution was dropped on to the surface of Fluorine doped Tin Oxide (FTO) substrate, which had an exposed area of 1.5 × 1.3 cm^2, and then dried under vacuum conditions for 1 h at 60 °C. This step was repeated five times to get uniform exposure of Ag(I)-CP on FTO. The resulting Ag(I)-CP photo anodes were used as working electrodes; a Pt wire was used as a counter electrode. The Ag/AgCl electrode was chosen as the reference electrodes. A 300 W-@ 1 Sun light intensity Xe lamp was used as the light source (Solar simulator: Bat Sol). The Mott–Schottky measurements were performed at frequency of 200-2000 Hz in the dark.

Computational method

The electronic structure of Ag(I)-CP was obtained using density functional theory (DFT) as implemented in Vienna *Ab initio* Simulation Package (VASP).[21,22] The interaction between the valence electrons and the core nuclei was approximated with the projector augmented wave (PAW) pseudopotential method.[23] In the calculations the valence electrons are expanded in terms of plane wave basis sets with an energy cutoff (E_{cut}) of 400 eV. The valence electronic configuration of the constituent atoms are as follows: Ag: [Kr] $4d^{10}$ $5s^1$, O: [He] $2s^2$ $2p^4$, C: [He] $2s^2$ $2p^2$ and H: $1s^1$. The Generalized Gradient Approximation (GGA) as parameterized by Perdew-Burke-Ernzerhof (PBE)[24] was used to calculate the exchange-correlation energy. GGA generally underestimates the band gap of a semiconductor and so, for better comparison with the experimental data, the band structure was also generated using HSE06 hybrid functional[25, 26] with a setting of 25% for the contribution from the short ranged Hartree-Fock exact exchange energy. The initial structure of the Ag(I) based polymer was taken from single crystal X-ray diffraction data (CCDC 198096). The unit cell of the Ag(I)-CP is composed of a simple monoclinic cell

with a total number of 36 atoms with composition $Ag_4C_{16}H_8O_8$, the structure is shown in Figure S18. The convergence criteria for energy and forces are taken to be ~ 10^{-5} eV and ~ 0.005 eVÅ^{-1}, respectively. The Brillouin Zone (BZ) is sampled by a mesh of 3×3×3 k-points generated by Monkhorst-Pack method.[27] The electronic structure has been smeared with a Gaussian of standard deviation 0.1 eV. The electronic band structure is generated after sampling the first BZ along high symmetry path Γ (G)—Z—D—B—Γ (G)—A—E—Z—C2—Y2—Γ (G), according to the recipe provided by Hinuma *et al*.[28] To estimate atomic charges Bader topological analysis[29, 30, 31] was employed.

In the Bader charge (BC) analysis, a surface is used to define the Bader region surrounding each atom of a compound from which charge density is assigned to that atom. The surface runs through the minima of the charge density in the location of the atom and the total charge for each atom is determined by integration of the electron density within the Bader region. The calculated Bader charges for the Ag(I)-CP are given in Table S1.

Evaluation of photocatalytic activity

Study on the water oxidation:

20 mg of the Ag(I)-CP catalyst and 10 mL of 0.01 M $AgNO_3$ *aq.* were loaded into a 50 mL two necked Pyrex glass vessel containing Ar. The resulting mixture was irradiated with UV light from a source of 250 W Hg lamps with gentle stirring. Hg lamp covers entire UV region (Xe lamp emits selective lines in UV region) and hence the Hg lamp was chosen for the entire photocatalytic process. The gaseous product (10 mL) was collected using an airtight syringe of 50 mL volume and analyzed by a GC (Thermo Fisher Scientific GC-Trace 1110) equipped with a TCD detector and a molecular sieve 5Å packed column. The reaction was also carried out without illumination (dark) keeping other experimental conditions unchanged.

The photocatalytic oxidation of Tartrazine, RhB and 2,4 DCP were studied using the following methodology:

20 mg of the prepared catalyst was placed in a one necked Pyrex glass vessel (30 mL) with mouth opened, which was then placed inside a photo reactor setup (an indigenously designed reactor by Lelesil Innovative System, India), maintained at a distance of 25 cm from the light source (250 W Hg lamp). Before light irradiation, the reaction vessel was placed in the dark and stirred for 30 minutes to allow the adsorption-desorption equilibrium between the pollutants (20 mL of 25 ppm) and Ag(I)-CP (1 mg/mL) to be established, thereafter the light was turned-on. During the progress of the reaction, 3 mL aliquots were collected at regular time intervals and centrifuged to remove the catalyst. The aliquots of tartrazine and 2,4 DCP were characterized by HPLC (Thermo Fisher Dionex UltiMate 3000 SD) using a diode array detector set to a wavelength of 452 nm for tartrazine and 284 nm for 2,4 DCP. The aliquots of tartrazine and RhB were also investigated separately using UV-Visible absorption spectroscopy (Thermo Scientific Evolution 201 UV−vis spectrophotometer). The degradation percentages for all the experiments are calculated using expression (1):

$$\text{Degradation (\%)} = (C_0 - C_t)/C_0 \times 100\% \quad (1)$$

Where C_0 and C_t are the concentration of the aliquots illuminated for 0 and t min, respectively. For comparison a study of the degradation of tartrazine was carried out using prepared semiconductor materials including Ag_2O, TiO_2, ZnO, and CuO by keeping other experimental conditions as similar.

Gas and Ion Chromatographic Details

The gaseous product (10 mL) from the degradation of tartrazine was collected by airtight syringe (50 mL) and analyzed by a GC (Thermo Fisher Scientific GC-Trace 1110) equipped with a FID detector and a molecular sieve 5Å packed column.

The ions present in the aqueous phase after photocatalysis (for degradation of tartrazine) were analyzed by an ion chromatograph (Thermo Fisher, Dionex ICS-2100 connected with a Software Chromeleon 7) equipped with Anion column- AS11, KOH as an eluent, using a run time of 12 min and Cation column - CS17, Methane Sulphonic Acid (MSA) as an eluent, using a run time of 20 min.

The GC-MS (Thermo Scientific Trace 1300 Gas Chromatography and ISQ single Quadrupole MS) and the LC-MS (Agilent 1200 infinity series LC and 6120 single quadrupole MS) of the product in the degradation of tartrazine in different time interval was carried out, the reaction mixture was first filtered to separate out the catalyst, then the remaining filtrate was extracted in ethyl acetate and filtered over anhydrous Na_2SO_4 to absorb water molecules. The organic solvent (EtOAc) was evaporated to dryness by a rotary evaporator. The dried product was dissolved in a minimum amount of acetonitrile, and analyzed by GC-MS and LC-MS.

RESULTS AND DISCUSSION

We accessed a facile precipitation route to synthesize nano-microstructure Ag(I) based coordination polymers with the spacer H_2bdc. Initially, possible binding modes of the organic linker bdc^{2-} to Ag^+ were evident from the FTIR spectra as shown in Figure S1a and it has been clear that the characteristic C=O stretching frequency was lowered from 1692 cm^{-1} (for free ligand) to 1580 cm^{-1} when carboxylate oxygen atoms are taking part in the coordination to the metal centre.[32] From the PXRD pattern (Figure 1a) of the prepared

sample, it was evident that the organic linker formed a binuclear species with the Ag(I) cation to give a monoclinic structure as the diffraction pattern of the sample is well indexed with the calculated pattern of binuclear Ag_2bdc species (CCDC 198096)[33].

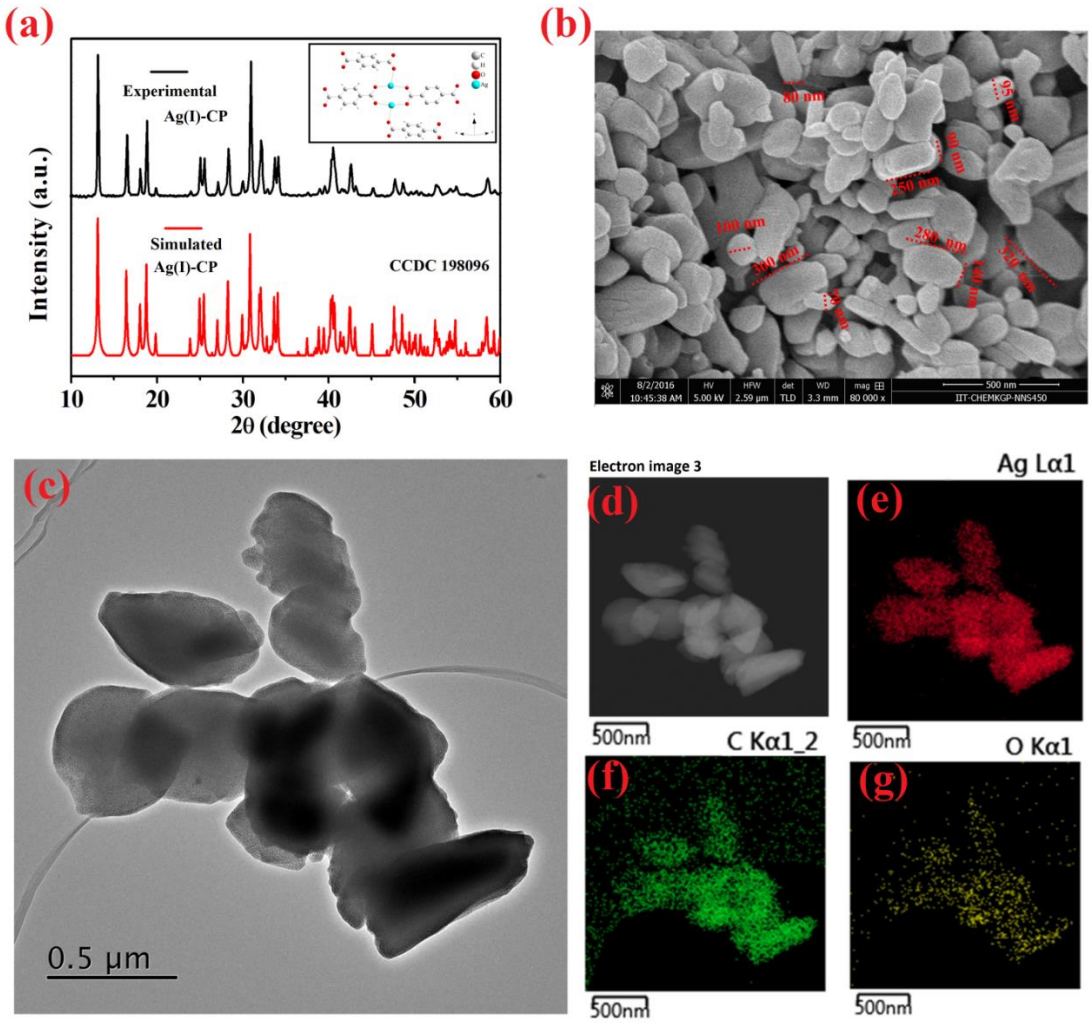

Figure 1. (a) PXRD pattern of prepared and simulated Ag(I)-CP (local structure of the CP shown in the inset) and (b) FESEM image, (c) TEM image of Ag(I)-CP with (d) STEM images and corresponding elemental mapping of (e) Ag, (f) C and (g) O.

No other phases of Ag(I) such as Ag_2O, Ag^0 are identified in the XRD pattern as verified from the comparison of characteristics XRD pattern of Ag_2O (JCPDS No: 41-1104), Ag^0 (JCPDS No:

04-0783) (Figure S1b). The detailed structure further reveals that, Ag(I) is coordinated with T-shaped geometry to the carboxylate oxygen atoms of the linker and that 1D chains are formed from the species through sharing bdc^{2-} ligands in a head-to-tail fashion, whereas each 1 D chain is connected others by weak Ag-O bonds, forming a 2D wave-like layer. The layers are connected to each other by Ag–O bonds of the other linker carboxylate μ^2–O of bdc^{2-} and form a 3D framework (Figure S2a and Figure S2b). In addition, an Ag-Ag interaction occurs in the 3D framework with a Ag-Ag distance of 2.9 Å (Figure S3b), which is significantly shorter than the Ag-Ag Van der Waals contact distance (3.40 Å).[33] Field Emission Scanning Electron Microscopic (FESEM) image (Figure 1b) and Transmission Electronic Microscopic (TEM) image (Figure 1c) showed that the aqueous precipitation process used to prepare these samples gives nano to micro size Ag(I)-CP. Further from elemental mapping profile it is obvious that uniform distribution of Ag, O, and C in the structure of CP (Figure 1d-1g). BET measurements give a moderate surface area of 39 m^2g^{-1} for the Ag(I)-CP materials and indicate a uniform pore size with average pore diameter of ~ 8.9 nm (Figure S4b). The chemical state of the elements present in the CP was verified using the XPS spectra shown in Figure 2a. The elements present in the CP are Ag, O, and C. The high resolution XPS spectra of Ag(3*d*) are shown in Figure 2b, and show the binding energies of $3d_{5/2}$ and Ag $3d_{3/2}$ states in these samples are 367.1 eV and 373.1 eV respectively, which is in good agreement with the literature values for Ag in the +1 oxidation sate.[17] The presence of the organic spacer in the sample was confirmed by binding energies of C-C (283.5 eV), C-O (285.0 eV), and C=C/C=O (286.9 eV) groups in the C 1*s* (Figure 2c).[34, 35]

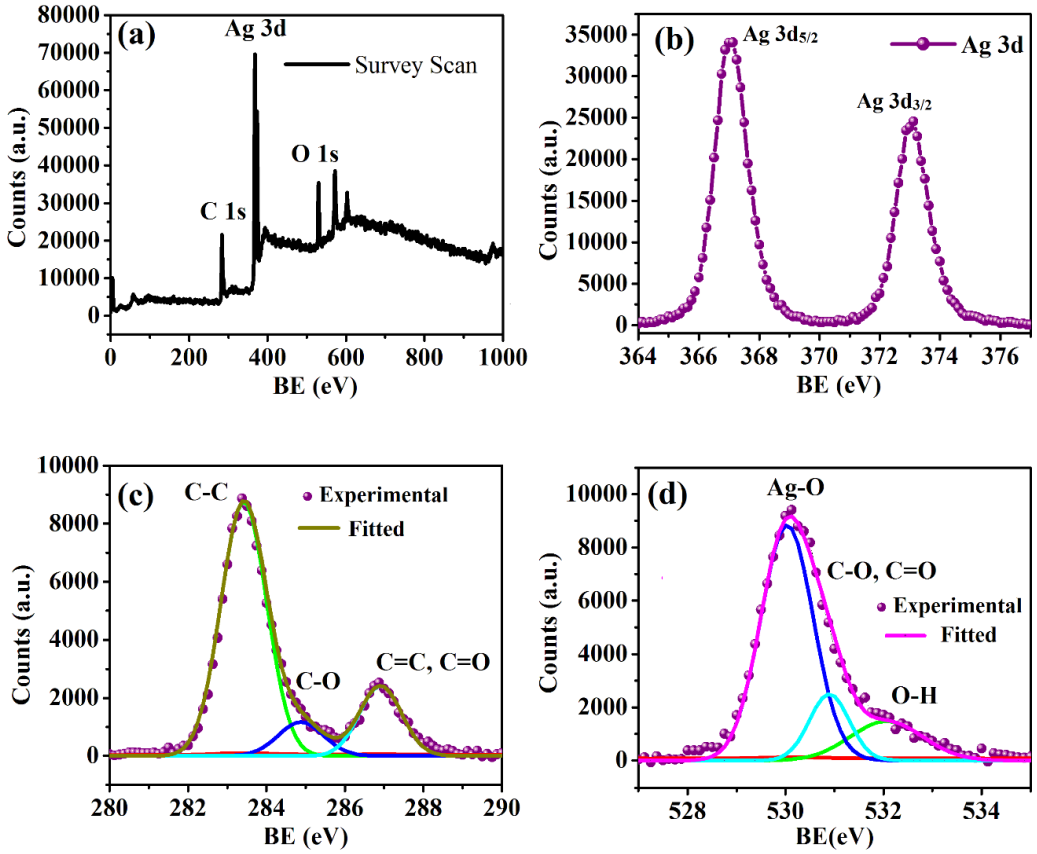

Figure 2. XPS spectra of surface elements of the prepared Ag(I)-CP: (a) Survey spectrum, (b) Ag element, (c) C element, (d) O element of Ag(I)-CP.

Solid state UV-visible absorption spectra of the free ligand H_2bdc and Ag(I)-CP were obtained and are shown in Figure 3a. Both show strong absorption in the wavelength range of 200 - 360 nm. However, the absorption of the free ligand in the region of 200-360 nm illustrate the feature of n→π* and π→π* transitions.[36] A hypsochromic shift of λ_{max} (~325 nm) assigned as a ligand centred transition was observed in the Ag(I)-CP due to loss of co-planarity of the phenyl ring and carboxylic moiety resulting from Ag-O bonding, as evidenced by the observed dihedral angle of ~ 22-23° for C3- C2- C1- O2 and O1-C1-C2-C4 (Figure S3a). In addition, a new weak shoulder peak located at 380 nm appeared in the low-energy region of the spectrum.

The Ag(I)-CP exhibits strong luminescence (Figure 3b) in the green region under irradiation by UV light which can be seen by the naked eye both in solid state and when the material is dispersed in water (Figure 3c). A solid-state luminescence study was carried out for the free ligand (λ_{ex} ~ 330 nm) and for the Ag(I)-CP material (λ_{ex} ~ 325 nm).

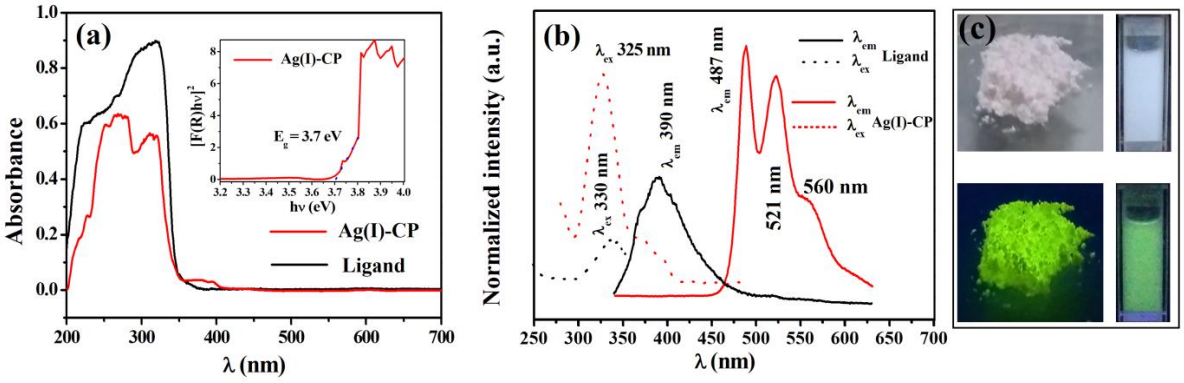

Figure 3. (a) UV-visible absorption spectra of free ligand (H_2bdc) and Ag(I)-CP (inset showing Kubelka-Munk plot for the CP), (b) photoluminescence spectra of free ligand (H_2bdc) and Ag(I)-CP upon excitation (λ_{ex}~325 nm for CP and λ_{ex}~330 nm for H_2bdc), and (c) photographs of the CP in solid state (left) and in aqueous dispersion (right) under daylight (above) and UV light (below).

Emission and excitation spectra of the free ligand and Ag(I)-CP are shown in Figure 3b, which shows a weak ligand centered emission ($\pi^* \rightarrow \pi$ transition) at 390 nm (λ_{ex} ~ 330 nm) in H_2bdc,[36] for Ag(I)-CP an intense radiative emission in the region of 460-600 nm (λ_{ex} ~ 325 nm) is observed. The emission in the higher wavelength region (460-600 nm) is expected due to a MLCT transition modified by metal-centered (d-s) states having Ag–Ag interactions.[37, 38]

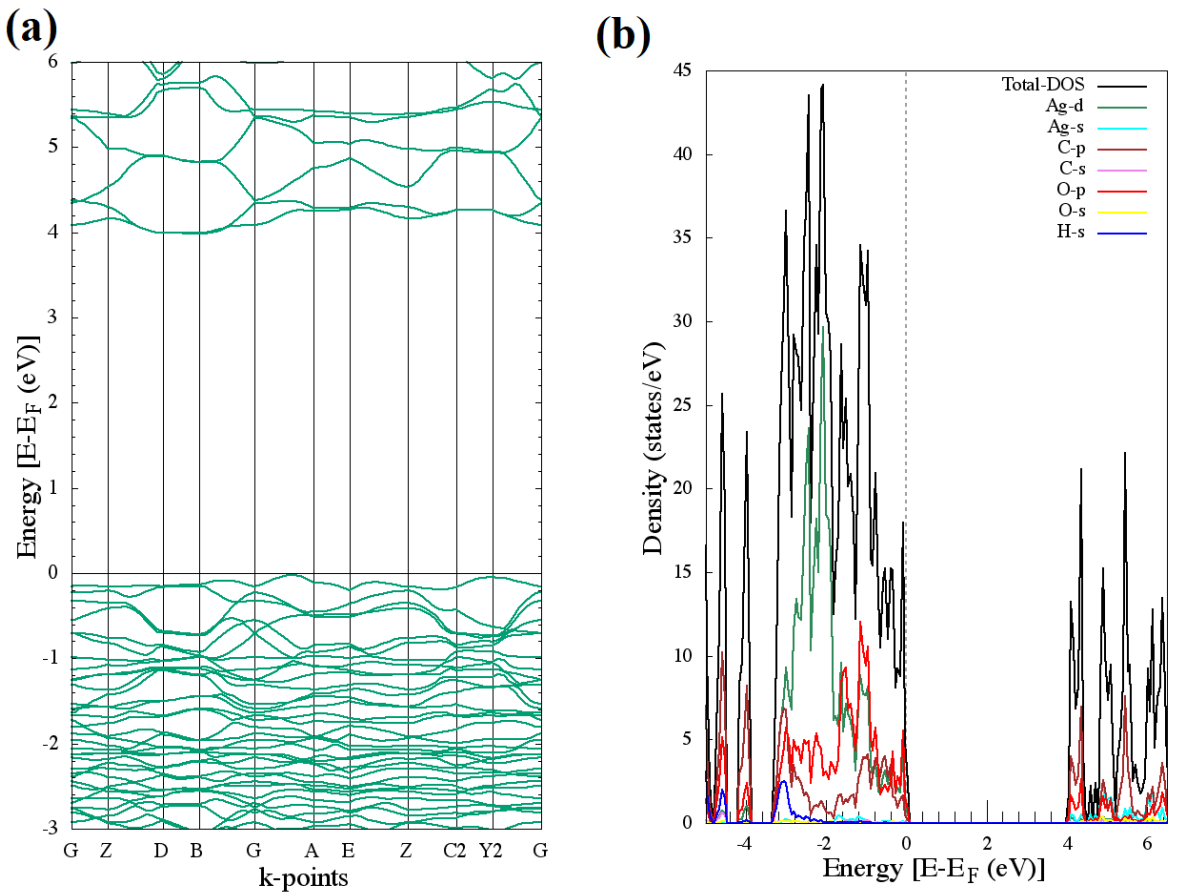

Figure 4. (a) Band structure, and (b) total density of states (black) and partial density of states (other colored area) of Ag(I)-CP using hybrid exchange-correlation HSE06.

In order to obtain a detailed electronic structure for Ag(I)-CP, the band structure and the density of states (DOS) of the Ag(I)-CP were calculated using hybrid density functional theory (HSE06), as implemented in the Vienna *Ab initio* Simulation Package (VASP). The band structure (HSE06) calculated along high symmetry special *k*-points is shown in Figure 4a. Equal energy valence band maxima (VBM) are located at Y2 and in between the Γ and A points. The conduction band minima (CBM) are at B and D. This means that the smallest indirect band gap (E_g) occurs with a calculated energy of 4.0 eV between VBM and CBM. However, the direct band gap at B and D is only 0.1 eV greater at 4.1 eV. This small energy difference suggests that

the Ag(I)-CP would mostly behave as a direct band gap material giving it higher quantum efficiency than would be expected for an indirect band gap material. The partial density of states (p-DOS) over a broader energy range is given in Figure S5, this reveals that Ag 4*d* orbitals are mostly confined between -4 to 0 eV (relative to the Fermi level), C 2*s* orbitals between -25 to -9 eV, while the 2*s* orbitals of O lie deep in the energy spectrum between -24 to -21 eV. The valence band maxima (VBM) is composed of an admixture of Ag 4*d* and O 2*p* orbitals with contribution from C 2*p* states (Figure 4b). On the other hand, the conduction band minima (CBM) have a majority of 2*p* states of C with some contribution from the corresponding 2*p* states of O (Figure 4b and Figure S5 and S6). Appearance of Ag *4d* and *5s* states at the CBM is also observed (as shown in Figure S6) as would be expected from the hybridization of Ag 4*d* and Ag 5*s*[39,40,41]enhanced by the short Ag-Ag contact (2.9 Å). However, the features for Ag 4*d* and 5*s* are less intense than those of C 2*p*. The electronic band structure obtained from the hybrid functional indicates a direct band gap of 4.1 eV. Experimental diffuse reflectance spectroscopy (DRS) was also used to estimate the band gap using the Kubelka-Munk plot approach. Figure 3a (inset) shows that the plot of $[F(R)h\nu]^2$ *vs* $h\nu$ for the Ag(I)-CP is nearly linear at the adsorption edge, indicating a direct transition, and extrapolation to the $h\nu$ axis gives a band gap estimate of 3.7 eV in close agreement with the band gap calculated from hybrid DFT. The band gap of 2.3 eV obtained from PBE functional calculations (Figure S7a) differs from the experimental value due to the well-known underestimation of the band gap in GGA-DFT, however the composition (Figure S7b) of the calculated hybridized states of orbitals in the valance band and conduction band, agrees well with the more accurate results obtained from the hybrid HSE06 method.[34]

The promising semiconducting properties of Ag(I)-CP prepared using the synthetic methods described earlier led us to test the photocatalytic performance of the material using, firstly, a

photoelectrochemical approach. An anode containing the CP was prepared following the procedure described in the methodology section. Figure 5a shows that, using the anode in an electrochemical cell, a photocurrent response was observed which followed the on-off cycle of illumination.

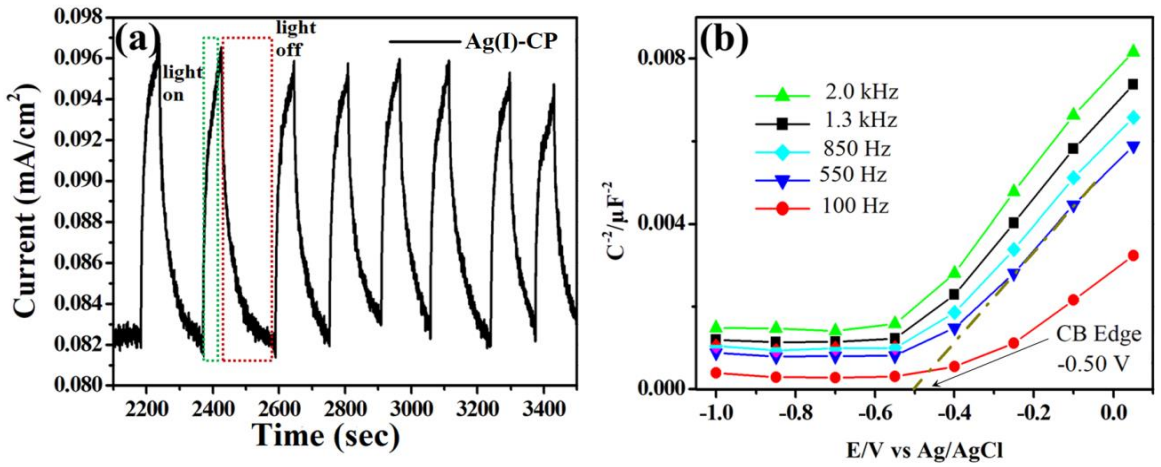

Figure 5. (a) Photocurrent response (300 W Xe lamps) of Ag(I)-CP in each on-off cycle, and (b) Mott-Schottky plots of Ag(I)-CP at different frequencies in 0.2 aq. Na_2SO_4 solutions (pH ~ 7).

This demonstrates that Ag(I)-CP is able to produce electron–hole pairs under light irradiation (300 W Xenon lamps). In general, Xe lamp emits light less in the region of UV. However a better photocurrent response could be achieved instead of Xe lamp if Hg lamp as light source would have used. The Mott-Schottky plot of reciprocal squared cell capacitance C^{-2} *vs* applied potential, *E* **(**Figure 5b**)** has a positive slope at all frequencies, which indicates that the as-prepared sample behaves as a typical *n*-type semiconductor.[42] The flat-band potential of the Ag(I)-CP is around -0.50 V *vs*. Ag/AgCl at pH 7, which is equivalent to -0.30 V *vs*. NHE at pH 7. The valance band potential of the Ag(I)-CP calculated from the optical band gap and the flat band potential is +3.40 V *vs.* NHE at pH 7, which highlights the highly oxidative nature of the

material and suggests that Ag(I)-CP could find applications in challenging oxidation processes, such as the removal of dye compounds from contaminated water.

The photocatalytic activity of the Ag(I)-CP was first assessed using the water splitting reaction using irradiation with a 250W Hg lamp. The production of O_2 as a function of time using the Ag(I)-CP as a photocatalyst was monitored by GC (Figure S8a). Background O_2 and N_2, which were present at levels of a few hundred ppm in the reactor, could not be excluded; thus, initially the O_2/N_2 volume ratio was considered for reliable qualitative understanding of O_2 generation.[43] As shown in Figure S8a**,** this ratio consistently increased with irradiation time, implying that O_2 was produced by the photocatalytic reaction of water under light irradiation. Whereas when a blank reaction (dark) was carried out, no change in the O_2/N_2 ratio was observed **(**Figure S8b).

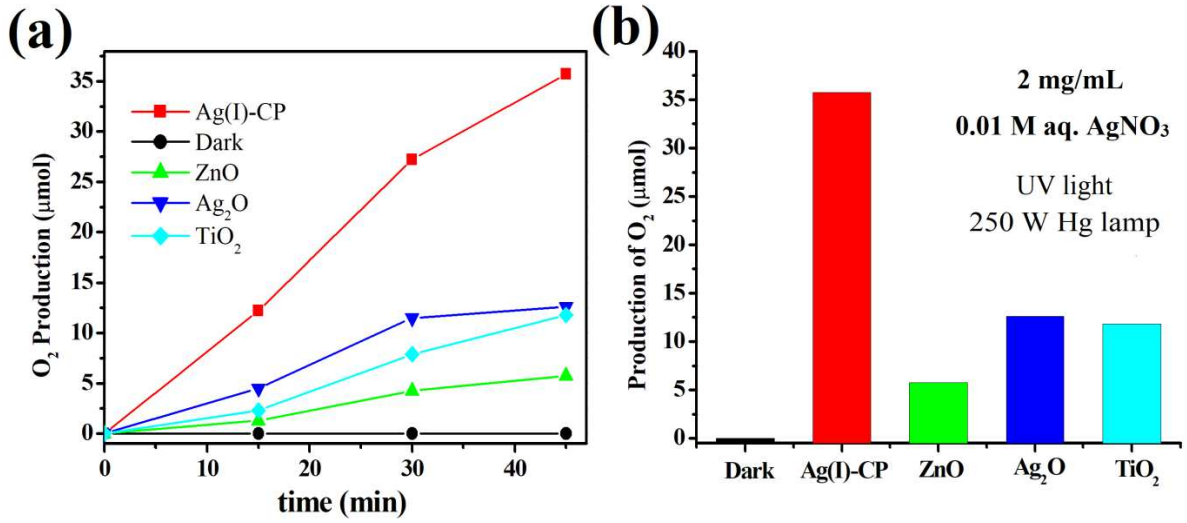

Figure 6. (a) Progress of photocatalytic O_2 evolution with respect to reaction time, and (b) a chart showing production of O_2 in dark and in presence of Ag(I)-CP, ZnO, Ag_2O, and TiO_2 under UV light (250 W Hg lamp) irradiation.

Further the quantitative estimation was done using calibration data in GC using mixture of standard gases (O_2, N_2 and H_2) in TCD detector. Subtracting the background O_2, the amount of

O_2 produced in presence of Ag(I)-CP is estimated as shown in Figure 6a. 35 µmol of O_2 is produced within 45 minute of UV light irradiation and in compare to prepared Ag_2O, TiO_2, ZnO, Ag(I)-CP shows better performance in O_2 production efficiency.

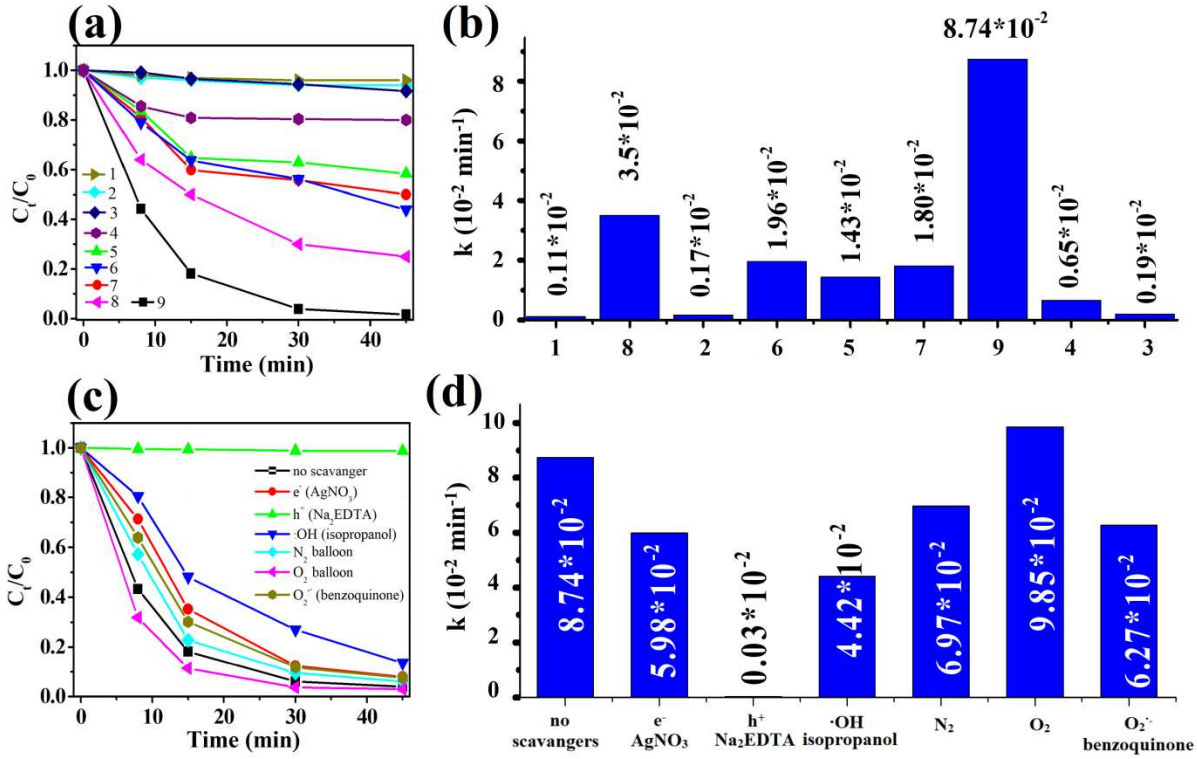

Figure 7. (a) Degradation plot (C_t/C_0 vs. time) of anionic tartrazine in presence of (1) (dark + Ag(I)-CP), (2) UV-Light (No catalyst), and (3) H_2bdc ligand, (4) $AgNO_3$ salt (0.05 mmol) (5) CuO, (6) TiO_2, (7) ZnO, (8) Ag_2O, and (9) Ag(I)-CP catalyst under irradiation of UV light (250 W Hg lamp), and (b) a chart showing their first-order rate constant value. (c) Effect of different quenchers and atmosphere on the photocatalytic degradation of tartrazine (C_t/C_0 vs. time) in presence of Ag(I)-CP, and (d) a chart showing their first-order rate constant value.

Notably, Ag(I)-CP shows 3 times better performance over Ag_2O (12 µmol), TiO_2 (11 µmol) and seven time better over ZnO (5 µmol) as presented in Figure 6b. To further test the oxidizing power of the photocatalytic system, we screen one model organic compounds: anionic tartrazine

azo dye (25 ppm) under UV irradiation (250 W Hg lamps). This represent important target compound for removal by oxidation as its presence in water causes hazardous pollution in the environment.[15,44,45] Before light irradiation, the reaction vessel containing (20 mL of 25 ppm) tartrazine and prepared CP (1 mg/mL) was placed in the dark and stirred for 30 minute to achieve adsorption-desorption equilibrium and Ag(I)-CP. Thereafter the light was turned on. During the progress of the reaction, 3 mL aliquots were collected at regular time intervals and centrifuged to remove the catalyst. The HPLC chromatogram (Figure S9) and UV-visible spectra (Figure S9; inset) of the supernatant solution in the subsequent process shows a gradual decrease of absorbance/peak area monitored at 428 nm indicative of dye degradation. Figure 7a shows that almost full degradation of initial tartrazine takes place within 45 min using the irradiated Ag(I)-CP as catalyst. An intermediate with mono substituted aromatic rings is obtained during the degradation process and this was also monitored via absorption at 354 nm (Figure S9).[45] Several intermediate molecules were identified by LC-MS and GC-MS during the degradation process as depicted in Figure S11, and Figure S12. Further, ion chromatographic and GC of the aqueous phase and gas phase reveals that the tartrazine is mineralizing into CO_2, H_2O, SO_4^{2-}, and NH_4^+ in presence of the CP photocatalyst (Figure S14-Figure S15; see supporting information Figure S13 for details of possible degradation pathways). To confirm that Ag(I)-CP does act as a photocatalyst for this reaction several additional tests were carried out and the results are included in Figure 7a. Firstly, tartrazine itself did not show self-degradation upon irradiation by the same light source (see also Figure S10a). Secondly, no tartrazine degradation is observed when Ag(I)-CP is included in the solution but without illumination, so that Ag(I)-CP does not show catalytic performance in the absence of light. We also found a very low rate of decomposition if the linker (ligand) alone was added to the

tartrazine solution (H_2bdc; ~0.2×10^{-2} min^{-1}). Similarly, use of a simple silver salt 0.05 mmol of $AgNO_3$(*aq.*), gave only a very slow degradation rate (0.65×10^{-2} min^{-1}) under the UV light, revealing a small photosensitization effect. To compare with other common photocatalysts Figure 7a also includes time online plots for the semiconducting materials mentioned in the Methodology section. In addition the relative rates for these materials and for Ag(I)-CP are compared in Figure 7b. The highest rate of degradation (~8.7×10^{-2} min^{-1}) was observed when Ag(I)-CP was employed as a photocatalyst, (Figure 7a, Figure 7b and Figure S10a). The calculated rate is found to be more than twice that of Ag_2O (~3.5×10^{-2} min^{-1}) and more than four times greater than alternative semiconductors not based on silver: ZnO (~1.8×10^{-2} min^{-1}), CuO (~1.4×10^{-2} min^{-1}), and TiO_2 (~1.9×10^{-2} min^{-1}).

To check on the mode of operation of the Ag(I)-CP photocatalyst, a series of quenching experiments were performed (Figure 7c). In the presence of a hole scavenger or with the inclusion of ·OH scavengers significant decreases in the rate of tartrazine degradation compared to the unmodified system were observed (rate = 3.0×10^{-4} min^{-1} with Na_2EDTA as hole scavenger and rate = 4.4×10^{-2} min^{-1} with isopropanol as ·OH scavenger). This suggests that photo generated h^+ and ·OH are the main active species that facilitate the tartrazine degradation process. There were also slight decreases in the measured tartrazine degradation rates observed in presence of $AgNO_3$ (e^- scavengers, rate = 5.9×10^{-2} min^{-1}), and benzoquinone BQ, ($O_2^{\cdot-}$ scavenger, rate = 6.2×10^{-2} min^{-1}), respectively (see Figure 7c; Figure 7d and Figure S10b). Hence, in addition to the main active species (h^+), electrons in the CBM (e^-) may also play a secondary role. This may also explain why a slight reduction in the rate (6.9×10^{-2} min^{-1}) was observed under a N_2 atmosphere, whereas the rate of the reaction was accelerated under an O_2 atmosphere (rate = 9.8×10^{-2} min^{-1}). Further, trapping experiments for hole and ·OH radical

were performed using TEMPO and coumarin as probes.[17,44,46] TEMPO is EPR active and hence samples using this quenching agent were also characterized using EPR spectroscopy (Figure 8a). The intensity of the signal corresponding to TEMPO was seen to gradually decrease with exposure to UV light in the presence of Ag(I)-CP, which infers oxidation of the TEMPO due to photo-generated holes.[17,46] The introduction of coumarin in another set of experiments gave a gradual increase of fluorescence intensity (Figure 8b), which can be attributed to the formation of ·OH adducts with the non-fluorescent coumarin molecules. This results in the generation of a fluorescent 7-hydroxy coumarin[44] and so the fluorescence intensity is found to increase gradually with respect to irradiation time due to the photocatalytic generation of ·OH radicals.

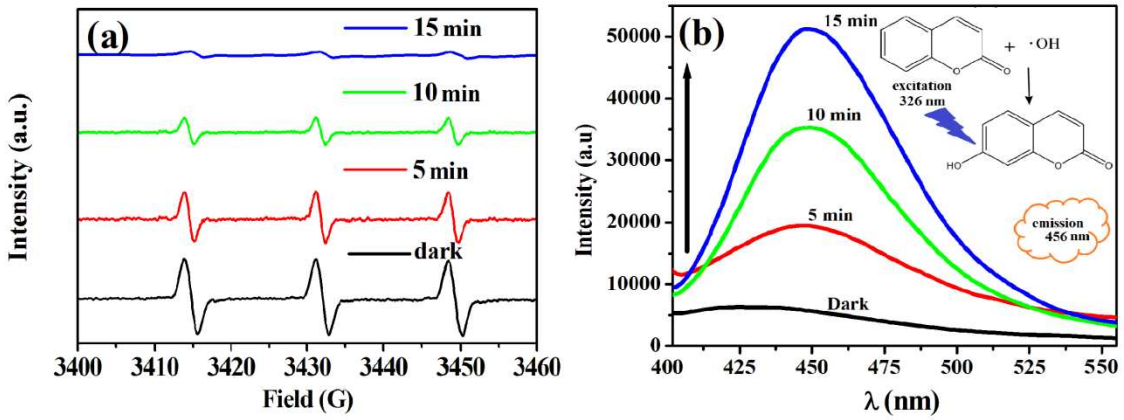

Figure 8. (a) Time dependent EPR spectra of TEMPO-h^+, and (d) fluorescence spectra of 7-hydroxy coumarin generated by ·OH radical adduct trapped by coumarin probe.

Hence, these quenching experiments confirm that the species mainly responsible for photocatalytic degradation of tartrazine into mineralized products are h^+ and ·OH. CP is also a promising material for the photo-oxidation of cationic RhB dye and chlorinated organic pesticides. Figure S16 and Figure S17a show the time dependent HPLC chromatogram of 2,4-

DCP and absorption spectra of RhB, respectively. Within 45 min, 84% of RhB is oxidized, with a calculated rate constant of 4.2×10^{-2} min^{-1}. About 78% of 2,4-DCP is dechlorinated within 45 min of starting the experiment, corresponding to a rate constant of 3.4×10^{-2} min^{-1} (Figure S17b and Figure S17c).

In order to more fully understand the high photocatalytic activity of Ag(I)-CP, the electronic density at the valance band and conduction band edges was also plotted to allow discussion of the likely charge transfer process resulting from photoexcitation. It can be seen from Figure 9a that electronic density near the VBM is located on the 4*d* orbitals of Ag^+ from the metal site and the 2*p* orbitals of O atoms and aromatic C atom in the linker molecules. While the electron density located at CBM is found on the carboxylate C atoms and on the C atoms in the aromatic region of the linker. This demonstrates that there is obvious charge transfer from Ag-O cluster from Ag_2O_4 unit of $Ag_2O_4C_8H_4$ species to π* of the ligand giving an M → π^* transition, *i.e.* MLCT.[47] However from Bader charges (shown in Table S1) for the atoms highlighted in the structure (Figure S18) revealed the Ag atoms in the structure have calculated Bader charges averaging ~ +0.75*e*, confirming the formal oxidation state assignment of Ag^+. C1-C4 (carboxylate carbon atoms attached to phenyl rings) have charges of +1.51*e* to +1.53*e* due to the strong bond polarization for C=O in carboxylate groups. Correspondingly, the charges calculated for the carboxylate O atoms (O1-O8) average –1.12 *e*. Aromatic carbon atoms (C5-C16) bear much lower charges (-0.06 to +0.15). Generally speaking, the more delocalized the electrons are in the covalent bond, the more conducive it is for charge transfer,[48] hence C=C being more covalent in character compared to C=O, Ag-O, favours LCCT $\pi\rightarrow\pi^*$ (process more efficiently rather than MLCT. In addition, we cannot exclude a little contribution of hybridised Ag (*d-s*) states at the CBM which resulted from M-M interaction, which includes a little admixture of

metal centre charge transfer as it was evident from luminescence behaviour of the CP (Figure 3b), however the majority of the CBM is formed by C *2p* states. The nature of the Ag–O bonding, Ag-Ag interaction does not affect the characteristics of the CBM significantly.[14,41,47]Hence, ligand centred charge transfer (LCCT) with admixture of MLCT modified by *d-s* state in the CP resulted in a generation of electron and hole in the active site. Further, the dispersive nature of the CBM, favors high mobility, allowing photo generated holes to migrate away from their production sites, which is important to allow the efficient production of free electrons and holes required for photo activity.

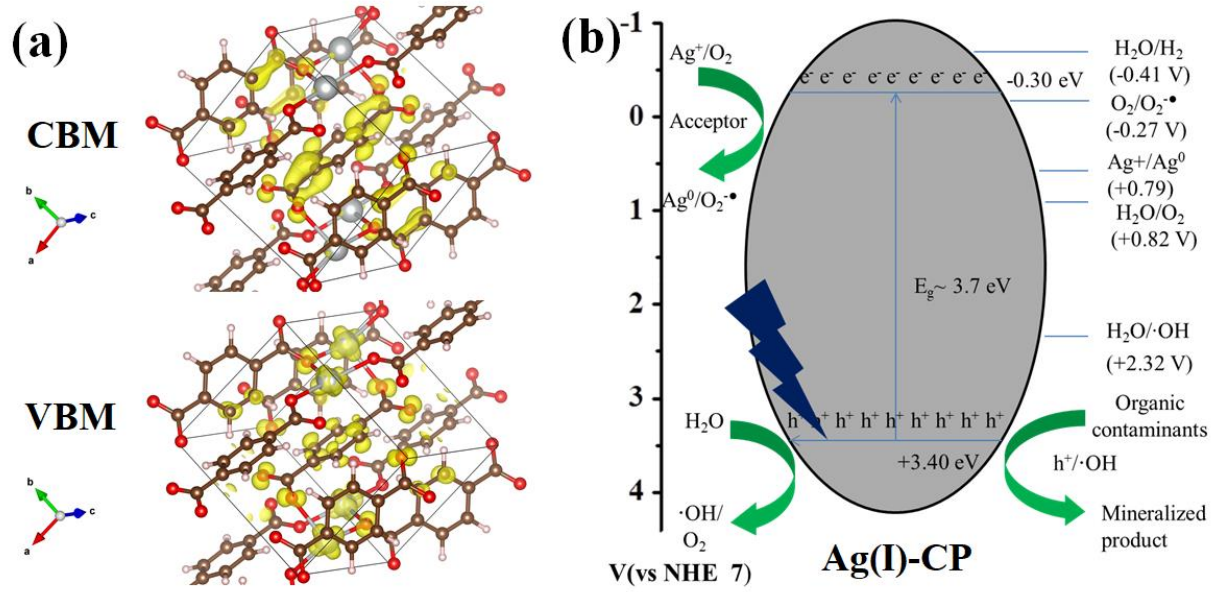

Figure 9. (a) Electron density at VBM (lower) and CBM (upper) of the Ag(I)-CP, and (b) UV light driven charge separation in the Ag(I)-CP and generated ROS responsible for OER and oxidation of model organic compounds such as tartrazine, RhB and 2,4 DCP.

Accordingly Ag(I)-CP is able to generate ROS (·OH) from an aqueous system, as holes (h^+) generated in the VB have a potential (+3.40V *vs* NHE) below the reduction potential for $H_2O/{\cdot}OH$ (+2.32V *vs* NHE at pH 7)[15,17]. This favours the production of oxidizing species

thermodynamically (Figure 9b). The position of the VBM edge of the CP (+3.40 V *vs* NHE is deeper than VBM (< +3 V *vs* NHE) of other common semiconductor systems such as TiO_2[49], ZnO[49], Ag_2O[44], and CuO[49]. Hence, this leads to the observed higher activity of Ag(I)-CP over the more conventional metal oxides. Nevertheless, the CBM is not low enough to produce H_2 from H_2O (-0.42 V *vs* NHE at pH 7), but the production of $O_2^{\cdot-}$ from O_2 (-0.27 V *vs* NHE) is favorable, because of thermodynamically permeable conduction band edge potential (-0.30 V *vs* NHE) of the CP system.[50, 51, 52] As we have shown, the generated hole (h^+) and free hydroxyl radicals from water/$O_2^{\cdot-}$are able to oxidize organic compounds such as tartrazine, RhB and 2,4-DCP to give mineralized products, following the steps (1-7) outlined below.

$$\text{Ag(I)-CP} + h\nu \rightarrow \text{Ag(I)-CP}\,(h^+ + e^-) \quad (1)$$

$$\text{Ag(I)-CP(s)} \rightarrow \text{Ag(I)-CP (aq)} \rightarrow 2Ag^+\,(aq) + bdc^{2-}\,(aq) \quad (2)$$

$$H_2O + \text{Ag(I)-CP}\,(h^+) \rightarrow \cdot OH + H^+ \quad (3)$$

$$OH\cdot + \text{Pollutants} \rightarrow \text{Degraded products} \rightarrow CO_2\,(g)\uparrow + H_2O \quad (4)$$

$$\text{Ag(I)-CP}\,(h^+) + \text{Pollutants} \rightarrow \text{Degraded products} \rightarrow CO_2\,(g)\uparrow + H_2O \quad (5)$$

$$\text{Ag(I)-CP}\,(e^-) + Ag^+\,(aq) \rightarrow Ag^0\,(s) \quad (6)$$

$$O_2(g) + \text{Ag(I)-CP}(e^-) \rightarrow O_2^{\cdot-} + 2H^+ + 2e^- \rightarrow H_2O_2 + e^- \rightarrow \cdot OH + {}^-OH \quad (7)$$

CP could be recycled and gives a photocatalytic efficiency of 93% in the 4th cycle (Figure 10a) for the photocatalytic oxidation of tartrazine. A little admixture of Ag *s* state hybridized with Ag *d* state in the CBM favours the reduction of lattice Ag^+ as observed in XPS (Figure 10b) and XRD pattern (Figure 10c) of used CP after photocatalysis.

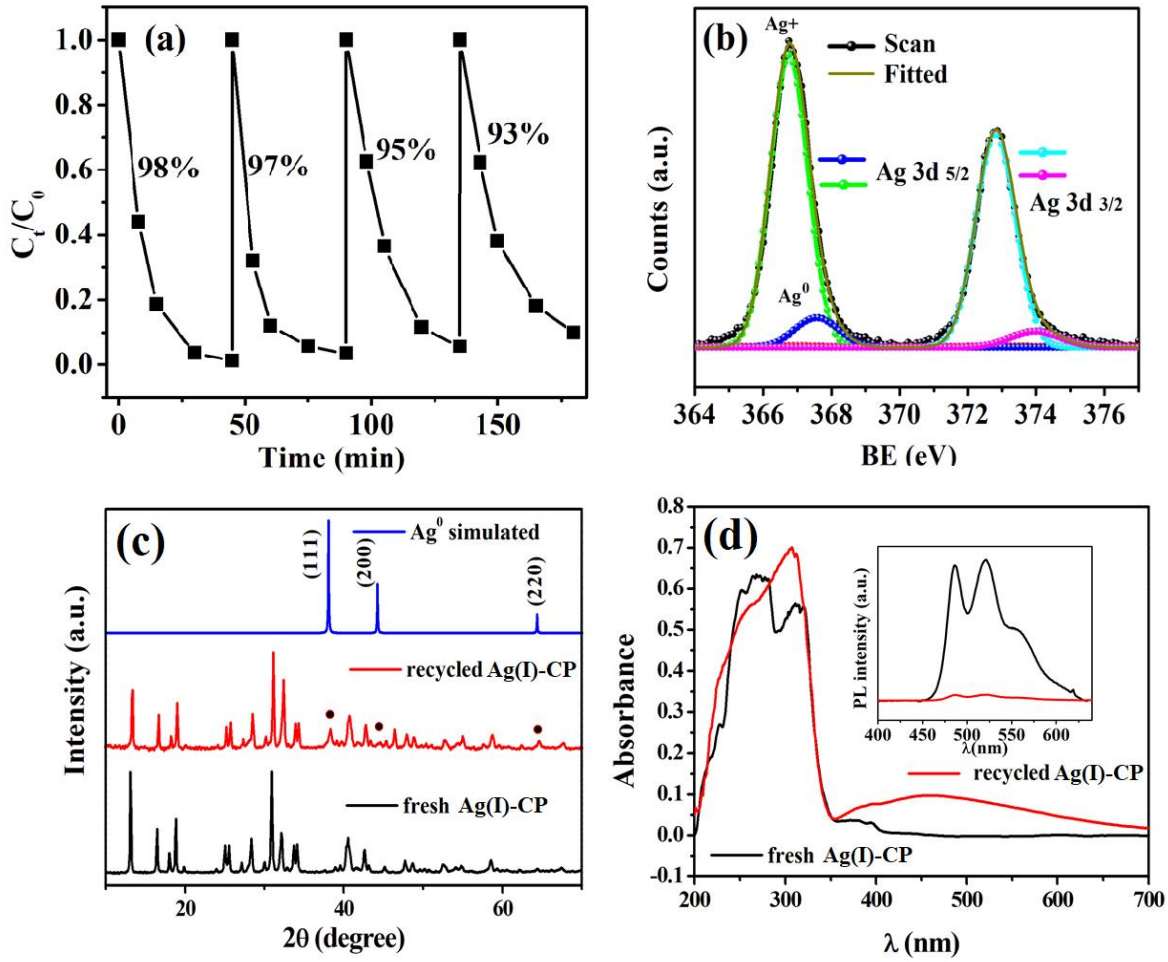

Figure 10. (a) Recyclability test of the Ag(I)-CP for the degradation of 25 ppm tartrazine under UV light irradiation for 4th cycle. (b) Ag 3*d* XPS spectra of used Ag(I)-CP photocatalyst. (c) PXRD patterns of the used (after 4th cycle) Ag(I)-CP and fresh Ag(I)-CP. (d) DRS spectra, and PL spectra (inset) of the used (after 4th cycle) and fresh Ag(I)-CP.

However, the states at the CBM are predominantly the π* orbitals of the organic linker and therefore, the reduction of atmospheric oxygen is preferred. Hence, the Ag(I)-CP exhibits less photo corrosion than other Ag based semiconducting systems as we have found the content of Ag^0 estimated by deconvolution of Ag 3*d* peak in XPS from this used Ag(I)-CP material is only

5.8 atomic% (Figure 10b, Figure S17d and Table S2). XRD analysis (Figure 10c) shows that the photocatalysts even after the 4^{th} cycle also retain its original Ag(I)-CP structure with a weak diffraction pattern corresponding to Ag^0. Figure 10d depict the comparison of DRS spectra of fresh and used Ag(I)-CP samples. Noticeably, the small percentage of Ag^0 deposited due to photo reduction of the Ag(I)-CP shows as a SPR band at around 440 nm (DRS spectra: Figure 10d), which disfavors the recombination process (PL spectra: Figure 10d; inset) shifts the light harvesting efficiency from UV to UV-Visible light.[13] Obviously, Ag(I)-CP is expected serve as a photocatalyst for oxidation of tartrazine in presence of simulated sunlight. Comparative studies on oxidation of tartrazine by Ag(I)-CP catalyst were carried out under different light irradiation conditions (refer Figure S19), such as UV light (250 W Hg lamp), simulated sunlight (250 W sun-photo lamp), and visible light (250 W tungsten lamp, $\lambda \geq 420$ nm). Since, the tartrazine itself absorbs light at λ_{max} = 428 nm and it could assist photocatalysis through self-sensitization process. However, the tartrazine degradation by our catalyst was minimum (~ 20%) under the visible light (shown in Figure S19). Overwhelmingly, the degradation efficiency of tartrazine by Ag(I)-CP was maximum (~ 98%) under the UV light irradiation. On contrary to the visible light, in presence of simulated sunlight the degradation efficiency of the dye had increased to moderate level (~ 42%), which is attributed by the combined effect of photocatalytic activity of Ag(I) CP (in UV light region) along with photo-sensitization of the dye (in visible region). Hence, combination of Ag(I)-CP with other semi-conductive/metal doped materials or organic sensitizers (in optimized composition) could serve as efficient visible light/sun light active photocatalytic systems, which will be a progressive research-topic investigated in near future.

CONCLUSIONS

In summary, we have presented nano-micro structured Ag(I)-CP as LCCT accompanied with MLCT based photocatalytic materials. Theoretical (hybrid DFT) and experimental evidence from DRS, PL and photoelectrochemical experiments support the behavior of Ag(I)-CP as new class of light active semiconductor. Ag(I)-CP was found to exhibit OER activity under UV light resulting from active hole generation from light induced charge separation. The material was successfully applied as a catalyst for the elimination of organic pollutants in aqueous solution. Ag(I)-CP could be readily recycled, maintaining high activity after four successive uses as a photocatalyst. The photocatalytic activity originates from the valance band position (hole) and conduction band position (e^-) of the material, which are capable of directly activating organic substrates via photogenerated h^+ or activating water and atmospheric oxygen, prompting oxidative elimination of the model compounds using $^{\cdot}OH$ radical species. In future, the morphology and band energy of the photocatalytic system (the CP exploited in this work) could be further engineered by tuning linker ligands or incorporating different metals in order to gain higher photoactivities for executing wide varieties of photocatalytic/photo-redox reactions.

ASSOCIATED CONTENT

The following files are available free of charge.

FTIR spectra, Comparison of XRD pattern with Ag and Ag_2O, 2D and 3D packing structure, and asymmetric unit present in the Ag(I) coordination polymer, XRD pattern of prepared metal oxide, N_2 adsorption-desorption isotherm, Electronic density of states (DOS/pDOS), Band structure (GGA-PBE& HSE06) of the CP. GC chromatogram for water oxidation and HPLC,

UV-vis absorption spectra, LCMS, GC for CO_2, GC-MS, Ion chromatograph for the degradation of tartrazine and first order kinetics plot. UV-visible absorption spectra of rhodamine B, HPLC of 2, 4 DCP, and kinetics plots for respective degradation. XPS spectra of the CP after used and Table of percentage of Ag^0 present in the Ag(I) coordination polymer. Table of Bader charges of the atom present in the coordination polymer.

AUTHOR INFORMATION

Corresponding Author

Dr. Rajakumar Ananthakrishnan,
Department of Chemistry, Environmental Materials & Analytical Chemistry Laboratory, Indian Institute of Technology, Kharagpur 721302, India
E-mail: raja.iitchem@yahoo.com; Fax: +91 3222-282252; Tel: +91 3222 282322

Notes

The authors declare no competing financial interest.

ACKNOWLEDGMENT

SM gratefully acknowledges the UGC, New Delhi for research fellowship. The authors acknowledge DST, New Delhi for FESEM and PXRD facilities (at Dept. of Chemistry, IITKGP) and XPS facility (at Dept. of Physics, IITKGP), Dr. A. Mukherjee, Environmental Science and Engineering, IIT KGP for Ion chromatographic analysis and finally, TEM analysis for revision (from School of Chemistry, Cardiff University, U.K). RA thanks the SERB, New Delhi (for HPLC-PDA). SPN acknowledges the support of the Supercomputing Wales project, which is part-funded by the European Regional Development Fund (ERDP) via Welsh Government and the ARCHER UK National Supercomputing Service (http://www.archer.ac.uk) *via* the membership of the UK's HEC Materials Chemistry Consortium.

ABBREVIATIONS

CP coordination polymer; ROS reactive oxygen species; RhB rhodamine B; 2, 4 DCP 2, 4 dichlorophenol; bdc^{2-} benzene dicarboxylate.

REFERENCES

1) Chang, K.; Li, M.; Wang, T.; Ouyang, S.; Li, P.; Liu, L.; Ye, J. Drastic Layer-Number-Dependent Activity Enhancement in Photocatalytic H_2 Evolution over $n$$MoS_2$/CdS ($n \geq 1$) Under Visible Light. *Adv. Energy Mater.* **2015**, *5*, 1402279.

2) Linsebigler, A. L.; Lu, G.; Yates, J. T. Photocatalysis on TiO_2 Surfaces: Principles, Mechanisms, and Selected Results. *Chem. Rev.* **1995**, *95*, 735-758.

3) Dhakshinamoorthy, A.; Asiri, M. A.; Garcia, H. Metal–Organic Framework (MOF) Compounds: Photocatalysts for Redox Reactions and Solar Fuel Production. *Angew. Chem. Int. Ed.* **2016**, *55*, 5414-5445.

4) O'Keeffe, M.; Yaghi, O. M. Deconstructing the Crystal Structures of Metal–Organic Frameworks and Related Materials into Their Underlying Nets. *Chem. Rev.* **2011**, *112*, 675-702.

5) Nasalevich, M. A.; Van der Veen, M.; Kapteijn, F.; Gascon, J. Metal–Organic Frameworks as Heterogeneous Photocatalysts: Advantages and Challenges. *CrystEngComm* **2014**, *16*, 4919-4926.

6) Alvaro, M.; Carbonell, E.; Ferrer, F. B.; Xamena, F. X. L.; Garcia, H. Semiconductor Behavior of a Metal-Organic Framework (MOF). *Chem. Eur. J.* **2007**, *13*, 5106-5112.

7) Dan-Hardi, M.; Serre, C.; Frot, T.; Rozes, L.; Maurin, J.; Sanchez, C.; Fe´rey, J. A New Photoactive Crystalline Highly Porous Titanium(IV) Dicarboxylate. *J. Am. Chem. Soc.* **2009**, *131*, 10857-10859.

8) Hendon, C. H.; Tiana, D.; Fontecave, M.; Sanchez, C.; D'arras, L.; Sassoye, C.; Rozes, L.; Mellot-Draznieks, C.; Walsh, A. Engineering the Optical Response of the Titanium-MIL-125 Metal–Organic Framework through Ligand Functionalization. *J. Am. Chem. Soc.* **2013**, *135*, 10942-10945.

9) Wu, X. P.; Gagliardi, L.; Truhlar, D. G. Cerium Metal-Organic Framework for Photocatalysis. *J. Am. Chem. Soc.* **2018**, *140*, 7904-7912.

10) Ji, M.; Lan, X.; Han, J.; Hao, C.; Qiu, J. Luminescent Properties of Metal–Organic Framework MOF-5: Relativistic Time-Dependent Density Functional Theory Investigations. *Inorg. Chem.* **2012**, *51*, 12389-12394.

11) Muhammad, U.; Shruti, M.; Kuang-Lieh, L. Semiconductor Metal–Organic Frameworks: Future Low-Bandgap Materials. *Adv. Mater.* **2017**, *29*, 1605071-1605075.

12) Gong, Y.; Shi, H. F.; Jiang, P. G.; Hua, W.; Lin, J. H. Metal(II)-Induced Coordination Polymer Based on 4‑(5-(Pyridin-4-yl)-4H-1,2,4-triazol-3-yl)benzoate as an Electrocatalyst for Water Splitting. *Cryst. Growth Des.* **2014**, *14*, 649-657.

13) Wang, F.; Li, F. L.; Xu, M. M.; Yu, H.; Zhang, J. G.; Xia, H. T.; Lang, J. P. Facile Synthesis of a Ag(I)-doped Coordination Polymer with Enhanced Catalytic Performance in the Photodegradation of Azo Dyes in Water. *J. Mater. Chem. A* **2015**, *3*, 5908-5916.

14) Martin, D. J.; Liu, G.; Moniz, S. J. A.; Bi, Y.; Beale, A. M.; Ye, J.; Tang, J. Efficient Visible Driven Photocatalyst, Silver Phosphate: Performance, Understanding and Perspective. *Chem. Soc. Rev.* **2015**, *44*, 7808-7828.

15) Jianting, T.; Yonghong, L.; Haizhu, L.; Zhen, T.; Datang, L. A Novel Ag_3AsO_4 Visible-Light-Responsive Photocatalyst: Facile Synthesis and Exceptional Photocatalytic Performance. *Chem. Commun.* **2013**, *49*, 5498-5500.

16) Zheng, C.; Yang, H. Assembly of Ag_3PO_4 Nanoparticles on Rose Flower-like Bi_2WO_6 Hierarchical Architectures for Achieving High Photocatalytic Performance. *J. Mater. Sci.: Mater. Electron.* **2018**, *29*, 9291.

17) Mandal, S.; Ananthakrishnan, R. Sustainable Design of Hierarchically Porous Ag_3PO_4 Microspheres through a Novel Natural Template and Their Superior Photooxidative Capacity. *ACS Sustainable Chem. Eng.* **2018**, *6*, 1091-1104.

18) Wang, X.; Li, S.; Yu, H.; Yu, J.; Liu, S. Ag_2O as a New Visible-Light Photocatalyst: Self-Stability and High Photocatalytic Activity. *Chem. Eur. J.* **2011**, *17*, 7777-7780.

19) Yoshida, R.; Suzuki, Y.; Yoshikawa. S. Syntheses of TiO_2(B) Nanowires and TiO_2 Anatase Nanowires by Hydrothermal and Post-Heat Treatments. *J. Solid State Chem.* **2005**, *178*, 2179-2185.

20) Georgekutty, R.; Seery, M. K.; Pillai, S. C. A Highly Efficient Ag-ZnO Photocatalyst: Synthesis, Properties, and Mechanism. *J. Phys. Chem. C* **2008**, *112*, 13563-13570.

21) Kresse, G.; Furthmüller, J. Efficient Iterative Schemes for *Ab-initio* Total-Energy Calculations Using a Plane-Wave Basis Set. *Phys. Rev. B* **1996**, *54*, 11169-11186.

22) Kresse, G.; Furthmüller, J. Efficiency of *Ab-initio* Total Energy Calculations for Metals and Semiconductors Using a Plane-Wave Basis Set. *Comput. Mater. Sci.* **1996**, *6*, 15-50.

23) Blöchl, P. E. Projector Augmented-Wave Method. *Phys. Rev. B* **1994**, *50*, 17953-17979.

24) Perdew, J. P.; Burke, K.; Ernzerhof, M. Generalized Gradient Approximation Made Simple. *Phys. Rev. Lett.* **1996**, 77, 3865-3868.

25) Heyd, J.; Scuseria, G. E. Hybrid Functionals Based on a Screened Coulomb potential. *J. Chem. Phys.* **2003**, *118*, 8207-8215.

26) Heyd, J.; Scuseria, G. E.; Ernzerhof, M. Erratum: "Hybrid Functionals Based on a Screened Coulomb Potential. *J. Chem. Phys.* **2006**, *124*, 219906.

27) Monkhorst, H. J.; Pack, J. D. Special Points for Brillouin-Zone Integrations. *Phys. Rev. B* **1976**, *13*, 5188-5192.

28) Hinuma, Y.; Pizzi, G.; Kumagai, Y.; Oba, F.; Tanaka, I. Band Structure Diagram Paths Based on Crystallography. *Comp. Mat. Sci.* **2017**, *128*, 140-184.

29) Bader, R. F. W. Atoms in Molecules: A Quantum Theory, Clarendon Press, Oxford, **1990**.

30) Henkelman, G.; Arnaldsson, A.; Jo´nsson, H. A Fast and Robust Algorithm for Bader Decomposition of Charge Density. *Comput. Mater. Sci.* **2006**, *36*, 354-360.

31) Guerra, C. F.; Handgraaf, J. W.; Baerends, E. J.; Bickelhaupt, F. M. Voronoi Deformation Density (VDD) Charges: Assessment of the Mulliken, Bader, Hirshfeld, Weinhold, and VDD methods for Charge Analysis. *J. Comput. Chem.* **2004**, *25*, 189-210.

32) Wang, G.; Liu, Y.; Huang, B.; Qin, X.; Zhang, X.; Dai, Y. A Novel Metal–Organic Framework Based on Bismuth and Trimesic Acid: Synthesis, Structure and Properties. *Dalton Trans*. **2015**, *44*, 16238-16241.

33) Sun, D.; Cao, R.; Bi, W.; Weng, J.; Hong, M.; Liang, Y. Syntheses and Characterizations of a Series of Silver-Carboxylate Polymers. *Inorg. Chim. Acta*. **2004**, *357*, 991-1001.

34) Jiang, H.; Zhou, P.; Wang, Y.; Duan, R.; Chen, C.; Song, W.; Zhao, J. Copper-Based Coordination Polymer Nanostructure for Visible Light Photocatalysis. *Adv. Mater.* **2016**, *28*, 9776-9781.

35) Wu, Y.; Luo, H.; Wang, H. Synthesis of Iron(III)-Based Metal–Organic Framework/Graphene Oxide Composites with Increased Photocatalytic Performance for Dye Degradation. *RSC Adv.* **2014**, *4*, 40435-40438.

36) Ma, J. F.; Jin, Y.; Shun-Li, L.; Shu-Yan, S.; Hong-Jie, Z.; Hai-Shui, W.; Kui-Yue, Y. Two Coordination Polymers of Ag(I) with 5-Sulfosalicylic Acid. *Cryst. Growth Des.* **2005**, *5*, 807-812.

37) Allendorf, M. D.; Bauer, C. A.; Bhaktaa, R. K.; Houka. R. J. T. Luminescent Metal–Organic Frameworks. *Chem. Soc. Rev.* **2009**, *38*, 1330-1352.

620 38) Han, L.; Yuan, D. K.; Wu, B. L.; Liu, C. P.; Hong, M. C. Syntheses, Structures and
621 Properties of Three Novel Coordination Polymers with a Flexible Asymmetrical
622 Bridging Ligand. *Inorg. Chim. Acta* **2006**, *359*, 2232-2240.

623 39) Sciau, P.; Kania, A.; Dkhil, B.; Suard, E.; Ratuszna, A. Structural Investigation of
624 $AgNbO_3$ Phases Using X-ray and Neutron Diffraction. *J. Phys. Condens. Matter*. **2004**,
625 *16*, 2795-2810.

626 40) Abrahams, S.; Bernstein, J. Crystal Structure of Piezoelectric Nonlinear-Optic
627 $AgGaS_2$. *J. Chem. Phys.* **1973**, *59*, 1625-1629.

628 41) Umezawa, N.; Shuxin, O.; Ye, J. Theoretical Study of High Photocatalytic
629 Performance of Ag_3PO_4. *Phys. Rev. B* **2011**, *83*, 0352021-0352028.

630 42) Gelderman, K.; Lee, L.; Donne, S. W. Flat-Band Potential of a Semiconductor: Using
631 the Mott–Schottky Equation. *J. Chem. Educ.* **2007**, *84*, 685-688.

632 43) He, Z. Q.; Wang, D.; Fang, H. Y.; Chen, J. M.; Song, S. Highly Efficient and Stable
633 $Ag/AgIO_3$ Particles for Photocatalytic Reduction of CO_2 under Visible Light.
634 *Nanoscale* **2014**, *6*, 10540-10544.

635 44) Yu, C.; Li, G.; Kumar, S.; Yang, K.; Jin, R. Phase Transformation Synthesis of Novel
636 Ag_2O/Ag_2CO_3 Heterostructure with High Visible Light Efficiency in Photocatalytic
637 Degradation of Pollutants. *Adv. Mater.* **2014**, 26, 892-898.

638 45) Al-Dawery, S. K. Photocatalyst Degradation of Tartrazine Compound in Waste Water
639 using TiO_2 and UV Light. *J. Eng. Sci. Technol*. **2013**, *8*, 683-691.

46) Rodr´iguez, N. A.; Parraab, R.; Grela, M. A. Structural Characterization, Optical Properties and Photocatalytic Activity of MOF-5 and Its Hydrolysis Products: Implications on Their Excitation Mechanism. *RSC Adv*. **2015**, *5*, 73112-73118.

47) Yanga, X.; Yan, D. Long-After Glow Metal–Organic Frameworks: Reversible Guest-Induced Phosphorescence Tunability. *Chem. Sci.* **2016**, *7*, 4519-4526.

48) Wang, G.; Sun, Q.; Liu, Y.; Huang, B.; Dai, Y.; Zhang, X.; Qin, X. A Bismuth-Based Metal–Organic Framework as an Efficient Visible-Light-Driven Photocatalyst. *Chem. Eur. J.* **2015**, *21*, 2364-2367.

49) Haque, F.; Daenekel, T.; Kalantar-zadeh, K.; Oul, J. Z. Two-Dimensional Transition Metal Oxide and Chalcogenide-Based Photocatalysts. *Nano-Micro Lett.* **2018**, *10*, 1-27.

50) Wood, P. M. The Redox Potential of the System Oxygen-Superoxide. *FEBS Lett.* **1974**, *44*, 22-24.

51) Miyauchi, M.; Nakajima, A.; Watanabe, T.; Hashimoto, K. Photocatalysis and Photoinduced Hydrophilicity of Various Metal Oxide Thin Films. *Chem. Mater.* **2002**, *14*, 2812-2816.

52) Li, X.; Yu, J.; Jaroniec, M. Hierarchical Photocatalysts. *Chem. Soc. Rev.* **2016**, *45*, 2603-2636.

660 **TOC Graphic**

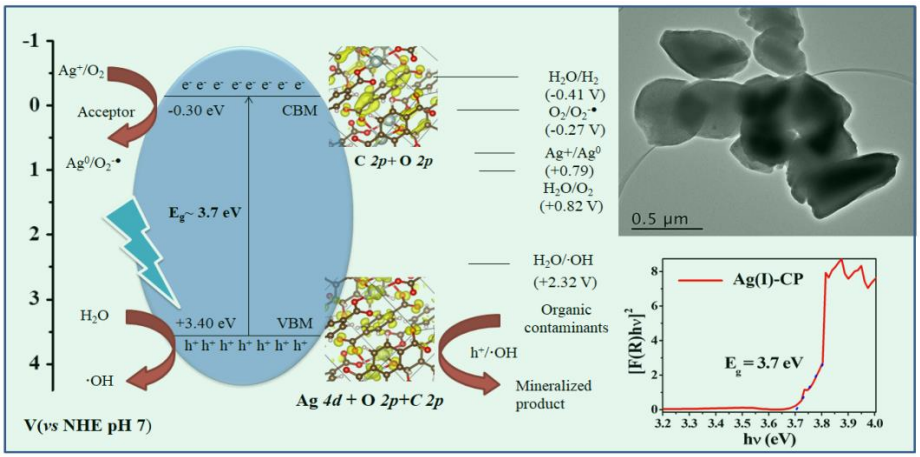

661